BIOCHEMISTRY
including biophysical chemistry & molecular biology
Article

Biochemistry **2009,** *48,* 12133–12144 12133
DOI: 10.1021/bi901480g

H135A Controls the Redox Activity of the Sco Copper Center. Kinetic and Spectroscopic Studies of the His135Ala Variant of *Bacillus subtilis* Sco[†]

Gnana S. Siluvai,[‡] Michiko M. Nakano,[‡] Mary Mayfield,[‡] Mark J. Nilges,[§] and Ninian J. Blackburn*[,‡]

[‡]*Department of Science and Engineering, Oregon Health and Science University, Beaverton, Oregon 97006 and* [§]*Illinois EPR Research Center, Urbana, Illinois 61801*

Received August 24, 2009; Revised Manuscript Received November 17, 2009

ABSTRACT: Sco-like proteins contain copper bound by two cysteines and a histidine residue. Although their function is still incompletely understood, there is a clear involvement with the assembly of cytochrome oxidases that contain the Cu_A center in subunit 2, possibly mediating the transfer of copper into the Cu_A binuclear site. We are investigating the reaction chemistry of BSco, the homologue from *Bacillus subtilis*. Our studies have revealed that BSco behaves more like a redox protein than a metallochaperone. The essential H135 residue that coordinates copper plays a role in stabilizing the Cu(II) rather than the Cu(I) form. When H135 is mutated to alanine, the oxidation rate of both hydrogen peroxide and one-electron outer-sphere reductants increases by 3 orders of magnitude, suggestive of a redox switch mechanism between the His-on and His-off conformational states of the protein. Imidazole binds to the H135A protein, restoring the N superhyperfine coupling in the EPR, but is unable to rescue the redox properties of wild-type Sco. These findings reveal a unique role for H135 in Sco function. We propose a hypothesis that electron transfer from Sco to the maturing oxidase may be essential for proper maturation and/or protection from oxidative damage during the assembly process. The findings also suggest that interaction of Sco with its protein partner(s) may perturb the Cu(II)−H135 interaction and thus induce a sensitive redox activity to the protein.

Sco1 is an essential accessory protein in the assembly of cytochrome *c* oxidase, the terminal enzyme of the respiratory chain. A large body of evidence links the function of Sco to the metalation of the Cu_A center in subunit 2 of the oxidase (Cox2). In both yeast and *Bacillus subtilis*, Sco mutant strains that impair or eliminate Cu binding produce a phenotype lacking in functional caa_3 oxidase, and high levels of Cu are able to rescue the caa_3 activity of *B. subtilis* Sco (BSco)[1] deficient strains (*1*−*6*). These data strongly implicate an interaction of the Cu-loaded BSco with the CtaC (Cu_A-containing) polypeptide as an essential element of caa_3 assembly and point to the transfer of copper from BSco to CtaC as a possible function (*3*). However, direct transfer of copper from Sco to Cox2 has not been demonstrated. In *Thermus thermophilus*, Sco was unable to transfer copper to Cox2 under conditions where transfer proceeded in a facile manner from the periplasmic copper binding protein PCuAC (*7*). Therefore, other functions for Sco proteins have been considered. The structural homology of Sco proteins to the thioredoxin family of thiol-disufide isomerases (*8*−*11*) has led to the hypothesis that Sco function is linked to thiol-disulfide redox (*9*, *11*) or redox signaling (*10*). More recent studies have identified thioredoxin-type activities for both BSco (*12*) and the PrrC homologue from *Rhodobacter sphaeroides* (*13*). The Cu_A center is known to form a disulfide between the two bridging thiolates in the apoprotein, and thioredoxin activity could conceivably be required to reduce the site to its copper-binding bis-cysteinate form. While the analogy to thioredoxins is attractive, the thiol-disulfide activity of BSco has been measured to be 80 times slower than that of thioredoxin itself (*12*). Wild-type (WT) BSco exists in stable form in both the Cu(I) and Cu(II) oxidation states (*14*), and the Cu(II) form shows no tendency toward autoredox to disulfide and Cu(I), although this chemistry was observed in a crystal of the Ni(II) derivative (*11*). These considerations suggest that Sco-type proteins may exhibit two or more distinct activities that include both copper transfer and redox activities.

To further understand the possible function of Sco proteins in vivo, our laboratory is exploring the structure−reactivity relationships of BSco and its homologues. A wealth of structural data is available on the metal binding sites of human and bacterial Sco1 proteins (*9*−*11*, *14*, *15*). NMR studies (*11*) have shown that Cu(I) binds to Cys169, Cys173, and His260 in the human protein (equivalent to C45, C49, and H135, respectively, in the *B. subtilis* protein), and this coordination is largely confirmed by EXAFS (*4*, *14*). NMR data for the Ni(II) state [a surrogate for Cu(II) binding] indicate a near-identical structure but with an extra oxygenic ligand derived from water or protein carboxylic side

[†]This work was supported in whole or in part by National Institutes of Health Grant GM54803 (to N.J.B.). This work was also supported at the Stanford Synchrotron Radiation Laboratory by the National Institutes of Health Biomedical Research and Technology Program, Division of Research Resources, and by the U.S. Department of Energy Office of Biological and Environmental Research. The Illinois EPR Research Center (IERC) is supported by the University of Illinois (Urbana, IL).

*To whom correspondence should be addressed: Division of Environmental and Biomolecular Systems, Department of Science and Engineering, Oregon Health and Sciences University, 20000 NW Walker Rd., Beaverton, OR 97006. Telephone: (503) 748-1384. Fax: (503) 748-1464. E-mail: ninian@comcast.net.

[1]Abbreviations: BSco, *B. subtilis* Sco; IPTG, isopropyl β-D-thiogalactopyranoside; WT, wild-type; NBT, nitroblue tetrazolium; BCIP, 5-bromo-4-chloro-3-indolyl phosphate; TMPD, *N*,*N*,*N*′,*N*′-tetramethyl-*p*-phenylenediamine; DTT, dithiothreitol; EDTA, ethylenediaminetetraacetic acid; EPR, electron paramagnetic resonance; EXAFS, extended X-ray absorption fine structure; XANES, X-ray absorption near-edge structure; PDB, Protein Data Bank.

Published on Web 11/18/2009

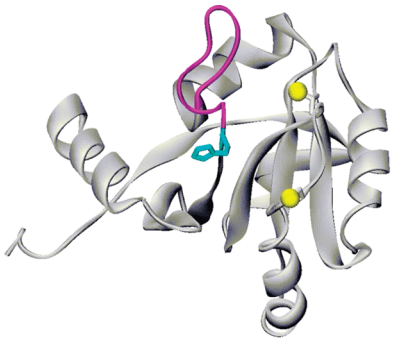

1	MGQQIKDPLNYEVEPFTFQNQDGKNVSLES	30
31	LKGEVWLADFIFTNCETICPPMTAHMTDLQ	60
61	KKLKAENIDVRIISFSVDPENDKPKQLKKF	90
91	AANYPLSFDNWDFLTGYSQSEIEEFALKSF	120
121	KAIVKKPEGEDQVIHQSSFYLVGPDGKVLK	150
151	DYNGVENTPYDDIISDVKSASTLK	

FIGURE 1: Structure and sequence information for *B. subtilis* Sco (BSco). One conformer of the NMR structure of the apoprotein (PDB entry 1ON4) is shown to illustrate the large separation between H135 (cyan) and the two Cys residues (C45 and C49, yellow) in the His-off configuration. The residues in the conformationally mobile loop 8 which is believed to interact with Cox2 are colored magenta (K121−H135). The bottom panel shows the sequence of the construct used in the paper with the residues color-coded to coincide with the graphical depiction of the structure.

chains completing the preferred four-coordinate geometry of the divalent cations (*11*). These metal-bound structures contrast with those of the apoprotein where the conformation of loop 8 which carries the coordinating His ligand is significantly perturbed and disordered such that the His ligand now resides some 10 Å from the metal center (Figure 1). Detailed analysis of the EXAFS data for the Cu(I) form of the *B. subtilis* protein suggested that Cu(I) coordination is best described by an equilibrium between His-on and His-off states, with the His-on conformer representing an occupancy of ~0.5 per Cu(I). Mutagenic analysis in yeast of residues located on the leading edge of loop 8 established a strong correlation with function, via abrogation of interaction of Sco with Cox2 rather than with Cox17 (*16*). Taken together, these data have led us to consider a hypothesis in which interaction of Sco with its partner via residues in loop 8 might induce a conformational transition between His-on and His-off states at the copper center, providing a "gated switch" mechanism for converting the protein between active and inactive states. This mechanism would predict different coordination and/or redox chemistry between His-on and His-off states.

To investigate this hypothesis, we have studied the structure and redox chemistry of the H135A variant of BSco. The properties of this variant differ in significant ways from those of the WT protein. We observe a remarkable increase in redox sensitivity when the H135 residue is replaced with a noncoordinating alanine residue that can be traced to a large decrease in the stability of the Cu(II) form. In contrast to previous studies (*4*, *12*), this variant binds copper but is susceptible to autoreduction of Cu(II) to Cu(I) (coupled to cysteine autoxidation to a disulfide) and exhibits a 10^3-fold increase in its reactivity toward hydrogen peroxide. Addition of imidazole causes EPR spectral changes consistent with rebinding of the imidazole ring to the Cu(II) center, yet this fails to fully restore the redox stability of the native Cu(II) form, suggesting a critical conformational role of the native H135 in stabilizing the Cu(II) state. These results support our hypothesis and suggest a mechanism in which binding of H135 to copper acts as a redox signal, capable of modulating the redox reactivity of the Sco protein. As part of this proposal, we suggest that interaction of Sco with its protein partner(s) may perturb the Cu(II)−H135 interaction and thus provide a sensitive redox switch induced by molecular recognition.

EXPERIMENTAL PROCEDURES

Construction of B. subtilis Sco Mutants. All *B. subtilis* strains used in this study are derivatives of strain JH642. The *sco* deletion mutant (*Sco*::*erm*) was constructed as follows. A 1.5 kb DNA fragment containing *Sco* (*ypmQ*) was amplified by polymerase chain reaction (PCR) from JH642 chromosomal DNA using oligonucleotides yq500RI [AGATGAATTCCCATTTGCTAATCTAATTTT (EcoRI site underlined)] and yq500Bam [AGATGGATCCTTCCTGAAACGGTTCAACGG (BamHI site underlined)]. The PCR product digested with EcoRI and BamHI was cloned into pUC18 digested with the same enzymes to generate pUC18-sco. To replace most of the *Sco*-coding region with an erythromycin-resistant (Erm^r) gene, pUC18-sco was digested with HpaI and EcoRV, treated with calf intestinal alkaline phosphatase, and ligated with the Erm^r gene isolated from pDG646 (*17*). The ligation mixture was used to transform *Escherichia coli* DH5α, and the transformants were selected for Erm^r. A plasmid isolated from the *E. coli* transformant was used to transform *B. subtilis* JH642. Chromosomal DNA was isolated from the Erm^r transformant (ORB6556) and was used as a template for PCR to confirm that ORB6556 resulted from the double-crossover recombination, which is indicative of the replacement of the *Sco* gene with the Erm^r gene.

Functional Analysis of the H135A Sco Mutant with a Complementation Assay. To determine whether the Sco (H135A) mutant is functional in vivo, the wild-type and mutant alleles of *Sco* were introduced into ORB6556 in trans as described below. The wild-type *Sco*-coding region as well as the promoter region was subcloned from pUC18-sco into the EcoRI−BamHI site of pDR111 (*18*), a plasmid used to integrate DNA into the *amyE* locus of the *B. subtilis* chromosome, to generate pDR111-sco. pDR111-sco was digested with HpaI and EcoRV, and the 520 bp *Sco* DNA fragment was replaced with the H135A mutant fragment that was isolated from the Sco (H135A)−intein fusion plasmid (described in the next section). After confirmation that the fragment was inserted in the right orientation, the plasmid was named pDR111-sco (H135A). Plasmids pDR111-sco and pDR111-sco (H135A) were used to transform ORB6556 (*Sco*::*erm*), and transformants were selected for resistance to spectinomycin (pDR111-derived) and erythromycin. Transformants that exhibited an amylase-negative phenotype were selected and named ORB6625 (*Sco*::*erm amyE*::*Sco*) and ORB6963 [*Sco*::*erm amyE*::*Sco* (H135A)].

A functional assay of the Sco (H135A) mutant was conducted via examination of cytochrome *c* oxidase caa_3 activity using a previously described TMPD oxidation method (*2*, *19*). In short, overnight cultures of JH642, ORB6556, ORB6625, and ORB6963 were appropriately diluted and plated onto a TBAB agar plate. After incubation at 37 °C for 2 days, the plates were kept at −20 °C for 10 min and tested for *N*,*N*,*N*′,*N*′-tetramethyl-*p*-phenylenediamine (TMPD) oxidation as described. TMPD-oxidase-positive clones turned blue.

Western Blot Analysis. The cell cultures of WT and H135A *B. subtilis* strains were grown in LB medium at 37 °C to a final OD_{600} between 0.6 and 0.8. For Western blot analysis, cells were broken in a French cell press and centrifuged at 6000*g*.

The supernatant containing both soluble and membrane fractions was solubilized in sodium dodecyl sulfate (SDS) buffer and separated on a gradient 8 to 16% SDS−polyacrylamide gel. After electrophoresis was performed, the proteins were transferred to a polyvinylidene difluoride membrane (Bio-Rad) in a wet blot using 25 mM Tris-glycine buffer in 20% (v/v) methanol. Anti-BSco rabbit serum obtained by immunizing rabbits with a purified BSco (Josman LLC) was used to recognize the WT and H135A variant. Antibodies were visualized by using the secondary antibody, goat anti-rabbit immunoglobulin G-alkaline phosphatase (AB applied biosystems) and a detection developer (Bio-Rad) containing a 1:1 mixture of nitroblue tetrazolium (NBT) and 5-bromo-4-chloro-3-indolyl phosphate (BCIP).

Cloning and Purification of BSco and Its His135 to Ala Variant. Wild-type BSco was purified from *E. coli* as described previously (*14*). Mutation of H135 to alanine in the wild-type BSco−intein fusion protein was performed via a transformer site-directed mutagenesis kit (Clonetech) (*20*), and its expression construct was confirmed by automated DNA sequence analysis. *E. coli* strain ER2566 (Novagen) carrying the mutant plasmid was grown in 1 L of LB-glucose medium containing 100 μg/mL ampicillin at 37 °C to a final OD_{600} between 0.6 and 0.8. The cells were treated with 500 μM IPTG for production of apoprotein, and the protein was purified following the earlier reported procedure (*14*). The isolated proteins were analyzed for protein concentration by Bradford assay, and their purity was checked by sodium dodecyl sulfate−polyacrylamide gel electrophoresis (SDS−PAGE) on an Amersham Biosciences PHAST system (20% homogeneous gel). When necessary, the protein was concentrated with an Amicon centricon ultrafiltration cell. The purified H135A protein was found to have a molecular mass of 19691.9 ± 1.9 Da (Figure S1 of the Supporting Information; the calculated mass with the two cysteines present as a disulfide is 19700 Da). The WT protein purified following the same procedure gave a mass value of 19756.6 ± 1.1 Da (Figure S2 of the Supporting Information). The difference in mass values is 64.7 Da, consistent with the theoretical difference between His and Ala substituents of 66.05 Da. The protein concentration was determined by absorption at 280 nm using an extinction coefficient of 19180 M^{-1} cm^{-1} (*9*), and this method resulted in a high yield of proteins for biochemical characterization (∼20−25 mg/L of culture). All chemicals and buffers used were reagent-grade and were obtained from the Fisher Scientific Co. or Sigma-Aldrich. Water was purified to a resistivity of 17−18 MΩ with a Barnstead Nanopure deionizing system.

Reconstitution with Cu(I) and Cu(II). Apoproteins were reduced anaerobically with 2 mM dithiothreitol (DTT). Excess DTT was removed by exhaustive dialysis in an anaerobic chamber. To obtain Cu(I)-loaded proteins, the WT and variant H135A proteins were reconstituted with tetrakis(acetonitrile)-copper(I) hexafluorophosphate as described previously (*14*). For Cu(II) reconstitution, proteins were loaded by in situ addition of 0.9 equiv of $CuSO_4$(aq) to the reduced apoprotein. In a similar way, the imidazole-bound Cu(II)−H135A complex was made by the in situ addition of 0.9 equiv of $CuSO_4$(aq) to a 1:1 mixture (per mole basis) of DTT-reduced apo-H135A and imidazole. The Cu(I)-reconstituted proteins were concentrated to a final volume of ∼1 mL and routinely analyzed for protein concentration with a Bradford assay. The copper content was measured by inductively coupled plasma optical emission spectrometry (ICP-OES) on a Perkin-Elmer Optima 2000 instrument.

Stoichiometry of Cu(II) Autoreduction. The thiol-reduced H135A apoprotein was incubated anaerobically with increasing amounts of $CuSO_4$(aq) from 1 to 4 equiv for 30 min. The excess Cu(II) added was removed through repeated exhaustive dialysis using 20 mM sodium phosphate buffer. The resultant autoreduced protein samples were concentrated using Amicon centricon filters (10 kDa cutoff), and their copper content was measured by ICP-OES.

Reactions with Hydrogen Peroxide. Reagent-grade hydrogen peroxide (30%, v/v; calcd concentration, 8.5 M) was purchased from Sigma-Aldrich. The concentrations of hydrogen peroxide working stock solutions (0.1−1 M) were measured from the absorbance at 240 nm using an extinction coefficient of 39.4 M^{-1} cm^{-1} (*21*). The reactivity of the Cu(II)−BSco complexes with hydrogen peroxide was followed spectrophotometrically at 23 °C by monitoring the decrease in absorption at 350−360 nm. Normally, 100 μM Cu(II)−protein complexes were used in all measurements in the presence of glucose (10 mM) and a catalytic amount of glucose oxidase (25 μg/mL reaction mixture) to ensure anaerobiosis (*22*). The Cu(II) chromophores decayed single-exponentially with time upon addition of hydrogen peroxide. A series of rates were calculated with varying hydrogen peroxide concentrations between 0.1 and 40 mM. The observed rates (k_{obs}) were plotted as a function of hydrogen peroxide concentration to yield the apparent rate constants (k_{app}). The evolution of dioxygen upon the reaction of hydrogen peroxide with the Cu(II) complexes of WT and H135A-BSco was measured at 23 °C using a Clarke-type dioxygen electrode (Rank Brothers, Bottisham, Cambridge, U.K.). The dioxygen electrode was calibrated with 20 mM sodium phosphate (Na-P) buffer at pH 7.2. At 23 °C, the atmospheric solubility of dioxygen in air-saturated 20 mM Na-P buffer (pH 7.2) was taken to be 240 μM. The electrode was calibrated with two points, pure argon (0 mA) and air-saturated buffer (200 mA). Hydrogen peroxide (1 M) was added anaerobically to 1 mL of WT and H135A-BSco, and the current produced upon the release of dioxygen was measured with time. From the value of the maximum current, the concentration of dioxygen released was calculated.

Reactions with Titanium(III) Citrate. Reagent-grade titanium(III) chloride was purchased from Sigma-Aldrich. Titanium(III) citrate was prepared by adding sodium citrate (0.875 mmol) to titanium(III) chloride (2.625 mmol) using a previously reported protocol (*23*). The concentration of titanium-(III) citrate was measured by spin quantitation of the X-band EPR spectrum using Cu(II)-EDTA as a spin standard. The reactivity of the Cu(II) complexes of WT BSco with titanium(III) citrate was followed spectrophotometrically at 23 °C by monitoring the decay in absorption at 445 nm using a Cary 50 spectrophotometer. H135A titanium(III) citrate kinetics were followed by sequential stopped-flow analysis using an Applied Photophysics SX-20 stopped-flow spectrometer. Apoprotein was first rapidly mixed with buffered $CuSO_4$(aq) to form the Cu(II)−H135A complex [Cu(II)−H135A] which was allowed to react for 2 s before being mixed with Ti(III) reagent, at which point data collection was initiated. Normally, 300 μM reduced apoproteins, 1 molar equiv of $CuSO_4$(aq), and 4 molar equiv of titanium(III) citrate were used in all measurements. The experimental data were fitted by nonlinear least-squares methods using DynaFit (*24*). Fit methods and parameters are given in Table S2 of the Supporting Information.

Spectroscopic Measurements. UV−vis spectra were recorded under anaerobic conditions in septum-sealed 1 cm

cuvettes using a Cary 50 spectrophotometer at 23 °C. For kinetic measurements, absorbance data were calculated at the desired wavelength with a time interval of 0.6 s. An Applied Photophysics SX-20 sequential stopped-flow spectrometer equipped with a rapid scanning photodiode array was used to conduct all the stopped-flow measurements at 23 °C. Spectra for quantitative EPR were recorded at X-band frequency on a Bruker Elexsys E500 spectrometer equipped with a Bruker ER049X SuperX microwave bridge, and a E27H lock-in detector. Temperature control was provided by a continuous nitrogen-flow cryostat system, in which the temperature was monitored with a Bruker W1100321 thermocouple probe. For EPR measurements on autoredox-sensitive H135A derivatives, anaerobic Cu(II) protein samples [100−500 μM in 20 mM sodium phosphate buffer (pH 7.2)] were prepared and frozen just prior to the EPR measurements. Spectra were recorded at 90 K under nonsaturating power conditions. The total spin due to Cu(II) was obtained by double integration and calibrated against a Cu(II)-EDTA standard curve at known concentrations (50−1000 μM) to give the number of Cu(II) atoms per protein. EPR experiments were also performed using enriched ^{65}Cu and ^{15}N imidazole to improve resolution for simulation. These spectra were recorded at X-band frequency on a Varian E-12 spectrometer. The temperature was kept at 110 K by a continuous nitrogen-flow cryostat system, and magnetic fields were calibrated with an NMR gaussmeter. EPR spectra were simulated using SIMPIPM, developed at the University of Illinois. SIMPIPM is the exact matrix diagonalization version of SIMPOW6 which is described in detail elsewhere (*25*). ^{65}Cu(II) samples were prepared by dissolving ^{65}CuO (Oak Ridge National Laboratory) in nitric acid and diluting appropriately in buffer before reconstitution.

Cu K-edge (8.9 keV) extended X-ray absorption fine structure (EXAFS) and X-ray absorption near-edge structure (XANES) data for the Cu(I)−H135A complex were collected on beamline 9-3 at the Stanford Synchrotron Radiation Lightsource operating at 3 GeV with currents between 100 and 80 mA as described previously (*26*). Monochromatic radiation was obtained via a liquid nitrogen-cooled Si[220] monochromator, and a Rh-coated mirror upstream of the monochromator (13 keV energy cutoff) was used to reject harmonics. The samples were measured as aqueous glasses in 20% ethylene glycol at 15 K. Data reduction and background subtraction were performed using the program modules of EXAFSPAK (*27*). Spectral simulation was conducted using EXCURVE version 9.2 as described previously (*14*, *28*−*30*).

RESULTS

Recombinant *B. subtilis* Sco (BSco) lacking the first 19-amino acid membrane-spanning domain was overexpressed in *E. coli* as described previously (*14*) to produce a final construct of 174 amino acids. The translated gene sequence of the expressed truncated protein is shown in Figure 1.

Formation of Cu(II) Complexes of the H135A Variant. For various biochemical studies, the soluble domain of BSco was expressed in *E. coli* and purified as reported previously (*14*). The H135A variant was constructed and purified by similar methods. Because the same conserved histidine variant (H239A) of yeast Sco1 was reported to barely bind Cu(I) [0.14 + 0.1 Cu(I)/protein] (*4*), the H135A-BSco variant was tested for its copper binding capacity. We found that the H135A variant still bound Cu(II). To quantify the amount of Cu(II) bound per H135A protein, the DTT-reduced protein was titrated with $CuSO_4$(aq) in steps of 0.25 molar equiv and monitored by the increase in absorption at 358 nm. This absorption is assigned to a thiolate to Cu(II) charge transfer transition and hence measures the extent of Cu(II) binding. The equivalence point at 0.95 Cu(II)/per protein suggests that H135A-BSco binds Cu(II) with a 1:1 stoichiometry (Figure S3 of the Supporting Information).

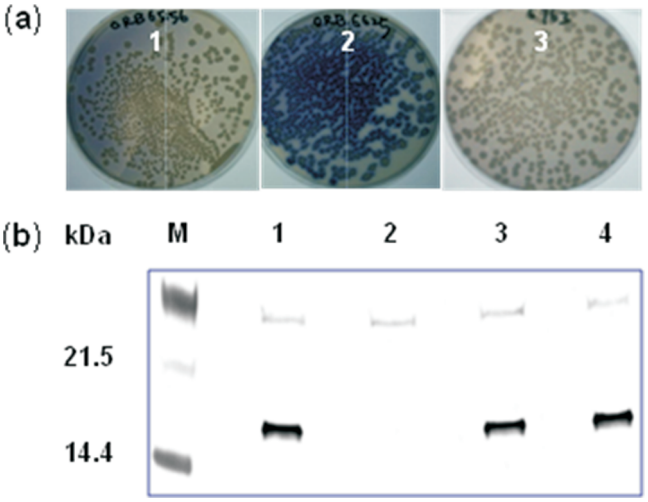

FIGURE 2: (a) Activity assay. Colony staining assay with the cytochrome caa_3-specific substrate TMPD. *B. subtilis* strains: ORB6556, *Sco*::*erm* (Sco deletion mutant) (1); ORB6625, *Sco*::*erm amyE*::*Sco* (Sco knockout complemented with the WT Sco gene) (2); and ORB6963, *Sco*::*erm amyE*:: *Sco*[H135A] (Sco knockout complemented with the H135A Sco gene) (3). (b) Western blot analysis of Sco expression in *B. subtilis*: lane 1, JH642 (WT); lane 2, ORB6556; lane 3, ORB6625; and lane 4, ORB6963 (*Sco*::*erm amyE*:: *Sco*[H135A]).

In contrast to the Cu(II)−WT protein complex, Cu(II)-bound H135A-BSco is unstable with respect to Cu(II) autoreduction (vide infra). Accordingly, imidazole was supplied as an exogenous ligand in an attempt to rescue the coordination of the conserved histidine and to restore the stability of the Cu(II) species. Imidazole was found to bind to the coordination sphere of the Cu(II)−H135A complex forming a Cu(II)−H135A-BSco+Imid adduct. Titration of a 1:1 mixture of the H135A variant and imidazole with $CuSO_4$(aq) gave an apparent Cu(II):protein ratio of 0.77 (Figure S3 of the Supporting Information), suggesting that the imidazole adduct of H135A is more susceptible to autoredox than the Cu(II)−H135A complex (since the disulfide form excludes the metal).

Abrogation of BSco Function in the H135A Derivative. To assess whether the amino acid substitution (H135A) affects the Sco activity in *B. subtilis*, we used the assay of colony staining with the cytochrome caa_3-specific substrate TMPD (Figure 2a, plate 1). Data establishing the abrogation of BSco function in H135A mutants have been reported previously (*2*) but interpreted in terms of the loss of copper binding ability. Since our H135A variant was still capable of binding copper, it was important to verify that the variant retained its nonfunctional phenotype. Our results confirmed those reported previously and showed that ORB6556 (*Sco*::*erm*) isTMPD oxidation-negative as expected whereas strains lacking the aa_3-600 quinol oxidase which lack the Cu_A center (*31*) were TMPD oxidation-positive (data not shown), suggesting that it is insertion of Cu_A into caa_3 that is defective in ORB6556. In ORB6625, where the wild-type *Sco* gene together with its promoter was integrated at the *amyE* locus of the *Sco* knockout mutant, TMPD oxidation ability was

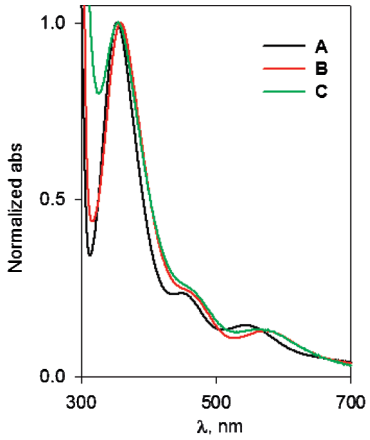

FIGURE 3: Optical absorption spectroscopy. Comparison of the normalized UV−vis absorption spectra of the H135A variant with WT BSco: Cu(II)−BSco (A), Cu(II)−H135A-BSco (B), and Cu(II)−H135A-BSco+Imid (C).

Table 1: UV−Vis Absorption Data for the Cu(II) Species of the WT and H135A Variant

complex	λ_{max} (nm) [ε (M^{-1} cm^{-1})]	$\varepsilon_{350}/\varepsilon_{450}$ ratio
Cu(II)−BSco	354 (6400), 450 (1385), 545 (865)	4.62
Cu(II)−H135A-BSco	358 (2800), 470 (690), 570 (400)	4.05
Cu(II)−H135A-Bsco+Imid	356 (3200), 470 (795), 560 (460)	4.03

restored (Figure 2a, plate 2). In contrast, the mutant *Sco* (H135A) gene was unable to complement the *Sco* knockout mutation (as shown in ORB6963), indicating that the H135A mutation results in the loss of cytochrome caa_3 activity (Figure 3a, plate 3). Therefore, H135A is nonfunctional but still binds copper stoichiometrically.

To confirm that the H135A mutation abrogates the cytochrome caa_3 activity by affecting copper insertion into the oxidase but not by affecting the level of the Sco protein, we next examined the intracellular levels of Sco by Western blot analysis (Figure 2b). The results showed that the level of Sco in ORB6925 and ORB6963 was similar and comparable to the level produced in the parental strain (JH642). This result indicated that the H135A mutation affects the function of Sco that is essential for the cytochrome caa_3 activity.

Spectroscopic Characterization. The UV−vis spectra of Cu(II)−H135A and its imidazole adduct in comparison with those of the WT are shown in Figure 3, with λ_{max}, ε, and peak intensity ratios given in Table 1. The spectral parameters differ somewhat from those of the WT protein but exhibit the same overall features, namely, a major absorption band likely due to S(Cys) 3pσ→Cu^{II} CT, a minor absorption band likely due to S(Cys) 3pπ → Cu^{II} CT, and a low-energy minor absorption band. The UV−vis spectrum is typical of tetragonal type 2 Cu thiolates in which the S p_σ transition (~350 nm) is more intense than the S p_π transition and occurs at a higher energy (*32*−*35*). The high-energy S p_σ interaction is dominant in tetragonal Cu(II) thiolates and occurs around 360−370 nm with extinction coefficients of ~5000 M^{-1} cm^{-1}; weaker S pπ → Cu(II) transitions occur to lower energies. The closest analogue of Cu(II)−BSco is nitrosocyanin, the red cupredoxin protein from *Nitrosomonas europa* which exhibits bands at 390, 496, and 720 nm similar in intensity to those in BSco (*35*−*37*). Like WT, the H135A derivatives have a unique intensity ratio of S(Cys) σ to S(Cys)π of ~4 but show small shifts in the λ_{max} values with a notable large drop in the extinction coefficient. The S(Cys) 3pσ → Cu(II) CT band exhibits a small red shift of 4 nm, and the low-energy band shows a larger red shift of 25 nm, in the following order: Cu(II)−WT BSco < Cu(II)−H135A+Imid < Cu(II)−H135A. The similarity of the UV−vis spectra of the H135A and WT proteins emphasizes the fact that the spectral features are dominated by the cysteinyl ligation and further suggests that the latter is not strongly perturbed in the H135A species.

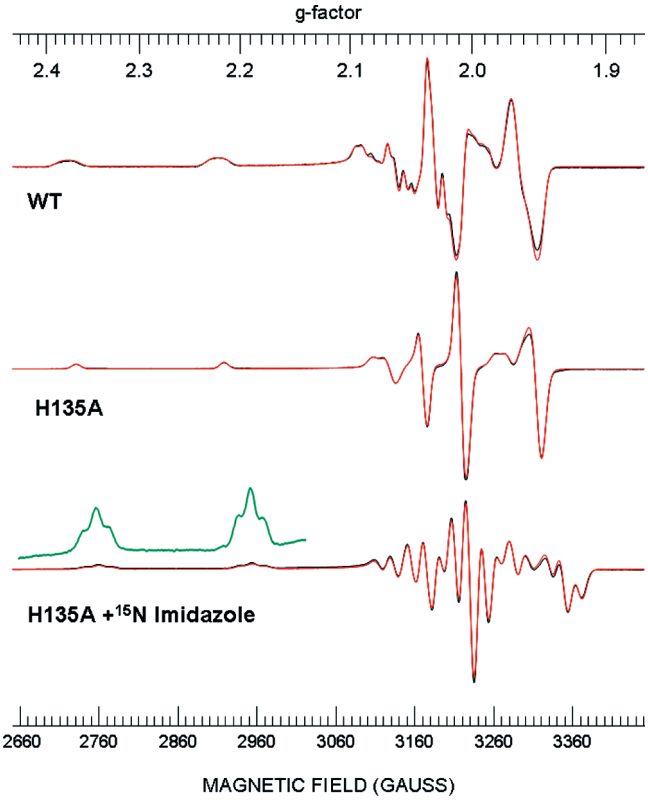

FIGURE 4: CW X-band EPR. Experimental (black) vs simulated (red) first-derivative X-band (9.395 GHz) EPR spectra of WT and H135A-BSco proteins: ^{65}Cu(II)−BSco (top), ^{65}Cu(II)−H135A-BSco (middle), and ^{65}Cu(II)−H135A-BSco with excess [^{15}N]imidazole (bottom). WT and H135A spectra are shown after exchange in D_2O which led to sharper line shapes (see the text). H135A+imidazole spectra are shown in H_2O since in this case no difference in line width was observed. The experimental parameters were as follows: center field, 3050 G; sweep width, 800 G; modulation amplitude, 2 G; modulation frequency, 100 kHz; number of scans, 30; temperature, 110 K; microwave power, 1.0 mW; microwave frequency, ~9.12 GHz.

EPR Spectra of H135A and Its Imidazole Adduct. Panels a and b of Figure 4 compare the first-derivative X-band CW EPR spectra of ^{65}Cu(II)−WT BSco and ^{65}Cu(II)−H135A-BSco (corresponding second-derivative spectra are shown in Figure S4 of the Supporting Information). In previous work (*14*), we reported EPR parameters of the WT protein as a nearly axial copper spectrum with a $g_\parallel$ of 2.15, a $g_\perp$ of 2.03, and well-resolved Cu hyperfine splittings. Second-derivative spectra were used to show the presence of resolved ligand superhyperfine structure that could be fitted by inclusion of nitrogen and/or proton splittings. Simulations showed that this structure was best accounted for with the hyperfine coupling of two spins, one ^{14}N (I = 1) and one proton (I = $^1/_2$), with the simulation parameters listed in Table 2. The ^{14}N coupling was further shown by ENDOR and ESEEM measurements to arise from a

Table 2: Simulated CW X-EPR Data[a] for the ^{65}Cu(II) Species of the H135A Variant in Comparison with the WT Species

	WT	H135A	H135A with [^{15}N]imidazole[c]	
g_x	2.0342(3)	2.0324(2)	2.0298(8)	2.0302(3)
g_y	2.0288(3)	2.0355(2)	2.0327(8)	2.0286(3)
g_z	2.1503(3)	2.1646(2)	2.1463(8)	2.1365(3)
$A_x(^{65}Cu)$	−135(2)	−145(2)	−129(5)	−143(2)
$A_y(^{65}Cu)$	−115(2)	−113(2)	−115(5)	−130(2)
$A_z(^{65}Cu)$	−572(2)	−569(2)	−560(5)	−584(2)
α^b	−11(2)	13(2)	−15(5)	−9(2)
β^b	1(1)	0(1)	0(2)	1(1)
γ^c	−12(3)	−	−	44(4)
$A_x(^{14}N1)$	30(1)	−	38(4) [54][d]	42(1) [58][d]
$A_y(^{14}N1)$	41(1)	−	27(4) [37][d]	34(1) [48][d]
$A_z(^{14}N1)$	31(1)	−	29(4) [40][d]	34(1) [48][d]
$A_x(^{14}N2)$	−	−	−	35(1) [49][d]
$A_y(^{14}N2)$	−	−	−	41(1) [58][d]
$A_z(^{14}N2)$	−	−	−	36(1) [50][d]

[a]Hyperfine principal values in megahertz (for units of 10^{-4} cm^{-1}, divide by 3). For equivalent ^{63}Cu hyperfine values, $A(^{63}Cu) = A(^{65}Cu)/1.0713$. Estimated error values given in parentheses. Line width and strain parameters are given in Table S3 of the Supporting Information. [b]Euler angles (convention of Rose) relating the noncoincidence between g and ^{65}Cu A principal axes. [c]Two species: 1:1 imidazole−Cu complex and 2:1 imidazole−Cu complex. [d]Calculated ^{14}N values are given. Measured ^{15}N hyperfine values are given in brackets.

coordinated histidine residue, while the ^{1}H coupling was assigned to one of the two coordinated cysteine ligands. The EPR spectra of the H135A variant are therefore expected to lack this strong N superhyperfine component. As shown in Figure 4, the perpendicular region of the spectrum of ^{65}Cu(II)−H135A lacks the superhyperfine splitting observed in that of the WT and can be simulated without any superhyperfine splitting, only ^{65}Cu splitting. The data clearly support the absence of histidine coordination in the H135A variant. Like Cu(II)−WT Bsco, Cu(II)−H135A-BSco showed some line narrowing when the sample was exchanged with D_2O, indicating the presence of a nearby exchangeable proton. Simulation parameters are listed in Table 2 and Table S3 (Supporting Information).

Next we asked the question of whether exogenous imidazole binding restores the WT EPR spectrum which would be an indication that imidazole should rescue the properties of WT BSco. When an excess amount of [^{15}N]imidazole was added to H135A, the low-field hyperfine line of the CW X-band spectrum showed the clear presence of a triplet splitting due to two nearly equivalent ^{15}N atoms, as shown (expanded view) in Figure 4c. However, careful simulation on multiple samples showed that the spectra could only be fitted by including both 1:1 and 2:1 imidazole−Cu(II) species. The simulation could be further improved if some of the unligated 0:1 imidazole (i.e., unbound H135A) was included in the fit. For the simulation in Figure 4c, the ratio of 2:1 to 1:1 to 0:1 was found to be 87:9:4. To confirm the existence of a 1:1 species, samples were prepared with differing molar amounts of [^{15}N]imidazole. Again it was found from fitting of the spectra (Figure S5 of the Supporting Information) that there is a mixture of all three species (Table 3) with the 1:1 species never being formed as a major (>50%) component. Unlike the unligated H135A, the 2:1 imidazole complex did not show any narrowing in line width upon exchange with D_2O but did show some increase in the amounts of 1:1 and 0:1 components. While our analysis shows that the chemistry of imidazole binding to the H135A variant is more complex than expected, there is no question that coordinated histidine is absent in the alanine variant

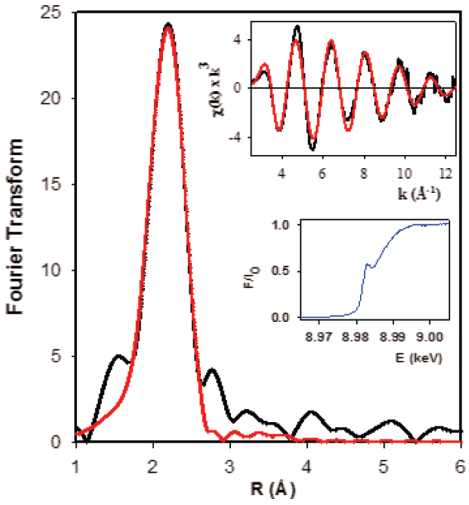

FIGURE 5: Cu K-edge X-ray absorption spectroscopy. Fourier transform, EXAFS, and absorption edge for Cu(I)−H135A. Black lines are experimental data, and red lines are simulated data. Parameters used in the simulations are listed in Table 3.

Table 3: Percentages of Components Obtained by Fitting Spectra as a Function of the Amount of Imidazole Added to Cu(II)−H135A-BSco

	percentage of spectral components		
	0.4 imidazole: Cu(II) ratio	0.8 imidazole: Cu(II) ratio	1.2 imidazole: Cu(II) ratio
spectral components			
0:1	66.3	45.1	29.6
1:1	27.8	38.6	41.3
2:1	5.9	16.3	29.1
imidazole:protein ratio (calcd)	0.40	0.71	1.0

and that addition of exogenous imidazole at a 1:1 stoichiometry gives rise to multiple speciation, no component of which accurately reproduces the WT EPR spectral features. The presence of a 2:1 imidazole−Cu(II)−H135A species further suggests that the WT Sco should bind a single imidazole as an exogenous ligand. As expected, addition of a slight excess of imidazole to WT BSco led to perturbation of the UV−vis spectrum to one similar to that formed from H135A with excess imidazole (Figure S6 of the Supporting Information). However, since the formation of an exogenous imidazole adduct with the WT protein is unlikely to have functional significance, it was not explored further.

X-ray Absorption Spectroscopy of Cu(I) Complexes. The Cu(I) coordination site structure of the Cu(I)- reconstituted sample of H135A-BSco was determined by X-ray absorption spectroscopy (Figure 5). The absorption edge shows a small peak at 8983 eV typical of three-coordinate Cu(I) (*38*). Fits to the EXAFS are listed in Table 4. High values of the Debye−Waller terms ($2\sigma^2$) were obtained when both Cu−S contributions were refined at the same distance (Table 4, fits A2 and B2) which may be due to structural inequivalence between the two Cu(I)−thiolate bonds. The parameters listed in fits A1 and B1 therefore represent the result of allowing the Cu−S shells to split. The splitting of Cu−S distances obtained from these simulations is lower than the resolution of the data ($\Delta R = \pi/2\Delta k = 0.14$ Å). Therefore, the data suggest but do not establish the presence of structural inequivalence between the two Cu−S interactions.

Table 4: Fits Obtained to the EXAFS of Reconstituted Cu(I)−H135A by Curve Fitting Using EXCURV Version 9.2

	copper EXAFS				
sample	scatterers[a]	distance[b] (Å)	Debye−Waller (Å)[c]	$-E_0$ (eV)	F[d]
fit A1	S	2.192	0.009	3.384	0.40
	S	2.274	0.008		
	0.6N	1.983	0.005		
fit A2	2S	2.234	0.011	3.172	0.39
	0.6N	1.972	0.005		
fit B1	S	2.206	0.007	4.964	0.40
	S	2.297	0.009		
	N	2.000	0.008		
fit B2	2S	2.245	0.011	4.46	0.41
	N	1.991	0.006		

[a]Coordination numbers are generally considered accurate to ±25%. [b]In any one fit, the statistical error in bond lengths is ±0.005 Å. However, when errors due to imperfect background subtraction, phase shift calculations, and noise in the data are compounded, the actual error is probably closer to ±0.02 Å. [c]Debye−Waller factors are listed as $2\sigma^2$. [d]F is a least-squares fitting parameter defined as $F^2 = (1/N)\sum^N k^6_{=1}(\text{data} - \text{model})^2$.

The best fit was found with two S donors and a third non-S ligand present at ~50% occupancy which could arise from solvent or residual acetonitrile carried over from the reconstitution protocol. Both the data and the simulation closely resemble those found previously for the Cu(I)-reconstituted form of the WT protein; in neither case was outer shell scattering from imidazole present in the FT, and no improvement to the fit was obtained by including multiple scattering contributions from outer shell C/N atoms of the imidazole ring. These data confirm the absence of the histidine side chain (as expected) in the Cu(I)−H135A-BSco EXAFS and also support our previous conclusion that the H135 side chain is only partially coordinated to Cu(I) in the fully reduced state of the WT protein (*14*). Given the essential nature of the H135 residue, this fact argues against the hypothesis that the Cu(I)−Sco complex is the active form as expected for a metallochaperone and points to a more complex role involving both oxidation states. Attempts to obtain EXAFS spectra for Cu(II)− H135A or its imidazole adducts gave data that were unreliable because of the tendency of these derivatives to undergo rapid photoreduction in the X-ray beam.

Analysis of the Autoreduction Reaction of Cu(II)−H135A. Sco proteins and their homologues are structurally similar to thioredoxins and peroxiredoxins (*39*, *40*), and because the Cu(II) complexes of the H135A variant of BSco are susceptible to autoreduction, we quantified the stoichiometry and the kinetics of the autoredox process. The copper content of the Cu(II)-reconstituted and subsequently autoreduced samples uniformly fell in the range of 58−65%, irrespective of the amount of added $CuSO_4$(aq) (Table S1 of the Supporting Information). Since the protein is completely bleached during the autoredox reaction, the 58−65% copper remains in the protein in the form of Cu(I), suggesting that two-thirds of Cu(II)−H135A undergoes autoreduction at the expense of two-electron dithiol to disulfide oxidation of one-third of Cu(II)−H135A to form one-third of apo oxidized H135A-BSco. The autoreduced Cu(I)−H135A-BSco did not reoxidize back to Cu(II)−-BSco in presence of air. The kinetics of Cu(II) autoreduction were determined from the spontaneous bleaching of the 358 nm absorption band and could be fit to a single-exponential kinetic process with a decay rate k of 1×10^{-3} s^{-1} (Figure S7 of the Supporting Information) at 1 equiv of copper addition.

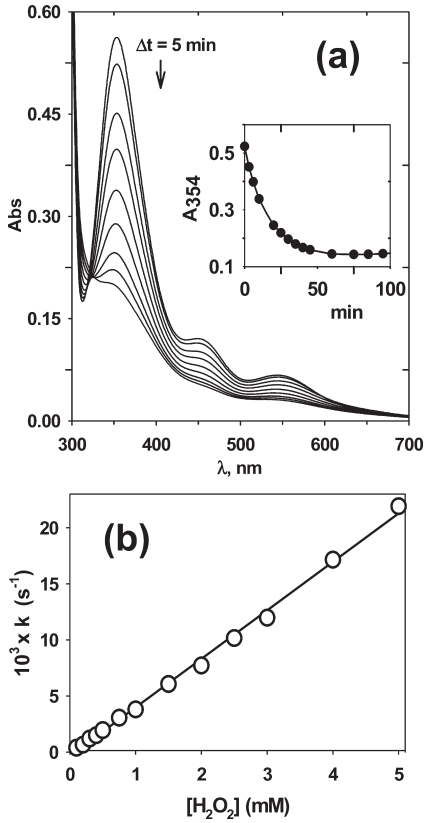

FIGURE 6: Reactivity of Cu(II)−WT BSco with H_2O_2. (a) Selected electronic absorption spectra showing the time-dependent changes associated with reduction of Cu(II)−WT BSco (100 μM) upon treatment with 1 equiv of hydrogen peroxide. The inset shows the single-exponential nature of the Cu(II)−BSco → Cu(I)−BSco reduction. (b) Linear dependence of first-order rates of Cu(II)−WT BSco (100 μM) reduction vs H_2O_2 concentration.

Reactivity with Hydrogen Peroxide. Williams et al. (*10*) reported that human Sco1 exhibited extreme sensitivity to hydrogen peroxide, but no kinetic data are available for the hydrogen peroxide reactivity for any of the Sco homologues (human, yeast, and bacteria). Therefore, we investigated the kinetics of the H_2O_2 reactivity of Cu(II)−WT BSco and compared it to that of the H135A variant and its imidazole adduct. The reactions were conducted under anaerobic conditions in the presence of a catalytic amount of glucose and glucose oxidase to consume any dioxygen generated during the course of the reaction and thus to maintain strictly anaerobic conditions. Proteins were reacted with peroxide at varying Cu:H_2O_2 ratios from 1 to 50. Upon addition of hydrogen peroxide, the red color of the protein was bleached with three visible absorption bands uniformly disappearing with time (Figure 6a). After the reaction was complete, the resultant colorless reaction mixture was concentrated by ultrafiltration (10 kDa cutoff), with several changes of 20 mM metal free sodium phosphate buffer to quantify the amount of copper remaining bound to the protein. Consistently, >65% of the copper remained protein-bound. The Cu(II)−BSco → Cu(I)−BSco reduction reaction induced by hydrogen peroxide follows a single-exponential kinetic process (Figure 6a, inset).

For the WT protein, a plot of k_{obs} versus peroxide concentration was linear with an estimated bimolecular rate constant of 4.2 M^{-1} s^{-1} (Figure 6b) with no evidence for saturation behavior up to 5 mM H_2O_2. For the H135A variant, however, different

kinetics were observed. The Cu(II) → Cu(I) reduction was a single-exponential kinetic process, similar to the hydrogen peroxide reactivity of Cu(II)−WT BSco (Figure 7a), but in contrast, the H135A variant showed saturation behavior at peroxide concentrations of ≤5 mM, suggesting the binding of hydrogen peroxide as a substrate at the Cu(II) site of the H135A variant (Figure 7b). The peroxide binding constant (K_A) was 3.9 mM, with a unimolecular rate constant of 2.6×10^3 s^{-1}. Remarkably, the overall rate of the reduction reaction is enhanced by 3 orders of magnitude compared to that of the WT protein.

The reaction of hydrogen peroxide with the imidazole adduct of H135A exhibits a linear dependence on peroxide concentration indicating kinetics similar to that of the WT protein. However, the plot of k_{obs} versus H_2O_2 concentration intersects on the *y* axis, indicative of a non-zero reduction rate in the absence of peroxide, consistent with the autoredox chemistry observed for this derivative (Figure 8).

For both WT and the H135A variant, the reduction of the copper center implies that peroxide is oxidized to dioxygen. To confirm this prediction, we measured the extent of dioxygen evolution during the reaction using an oxygen electrode. The results are shown in Figure 9. When Cu(II)−WT BSco (800 μM) was reacted with 10 equiv of hydrogen peroxide, the current produced (306 mA) corresponded to 367.2 μM O_2 (~38%). Similarly, when Cu(II)−H135A-BSco (500 μM) was reacted with 1 equiv of hydrogen peroxide, the current produced (116 mA) corresponded to 139.2 μM O_2 (~26%). Therefore, the reaction with peroxide generates dioxygen in both cases and confirms that the peroxide is oxidized in the process.

Reaction with One-Electron Redox Agents. The results obtained for peroxide reduction of BSco suggest that the peroxide forms an inner sphere complex with the H135A variant BSco, by coordinating to a vacant coordination position. The question of whether this reactivity is specific to peroxide or whether the copper centers are reducible by one-electron outer sphere reductants arises. Therefore, WT BSco and the H135A derivative were reacted with the one-electron reductants potassium ferrocyanide and titanium(III) citrate. Potassium ferrocyanide ($E^0 \sim 400$ mV) did not reduce the WT protein at an observable rate but did reduce H135A. To quantify the difference in reduction rates between WT and H135A, we used a lower-potential reductant ($E^0 \sim -650$ mV), Ti(III) citrate. To prevent Cu(II) autoreduction, apoprotein was first reconstituted by rapid mixing with Cu(II)(aq) in the stopped-flow apparatus and allowed to react for 2 s prior to being mixed with the Ti(III) citrate reagent. Data obtained from stopped-flow spectro-kinetic measurements were fit using DynaFit, and the fit procedures and parameters are described in the Supporting Information (Table S2 and Figure S8). WT protein was reduced in a slow bimolecular

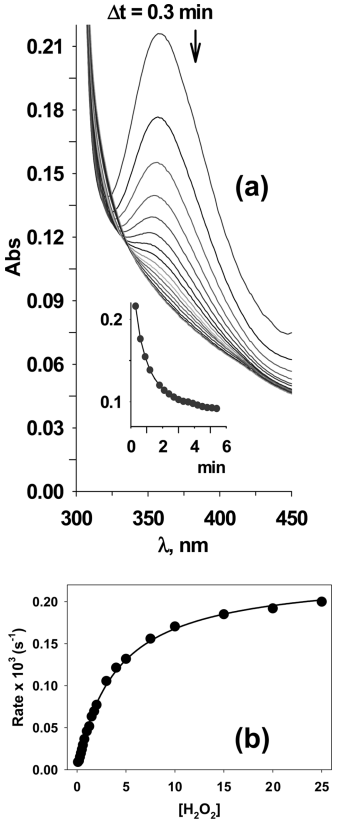

FIGURE 7: Reactivity of Cu(II)−H135A-BSco with H_2O_2. (a) Selected UV−vis kinetic traces showing the time-dependent changes associated with reduction of Cu(II)−H135A-BSco (100 μM) upon treatment with 1 equiv of hydrogen peroxide. The inset shows the single-exponential nature of the Cu(II)−H135A-BSco → Cu(I)−H135A-BSco reduction. (b) Nonlinear plot of the first-order rate of Cu(II)−H135A-BSco reduction vs H_2O_2 concentration fitted to the Michaelis−Menten equation.

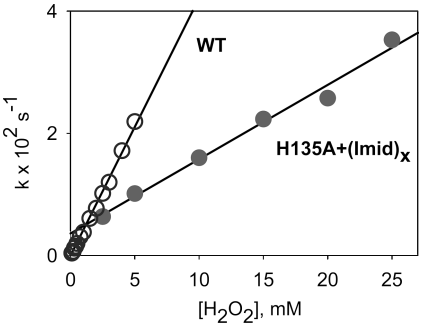

FIGURE 8: Reactivity of Cu(II)−H135A-BSco with H_2O_2 in the presence of imidazole. Linear dependence of the first-order rate of reduction of Cu(II)−H135A-BSco+Imid (100 μM, 1 molar equiv) vs H_2O_2 concentration.

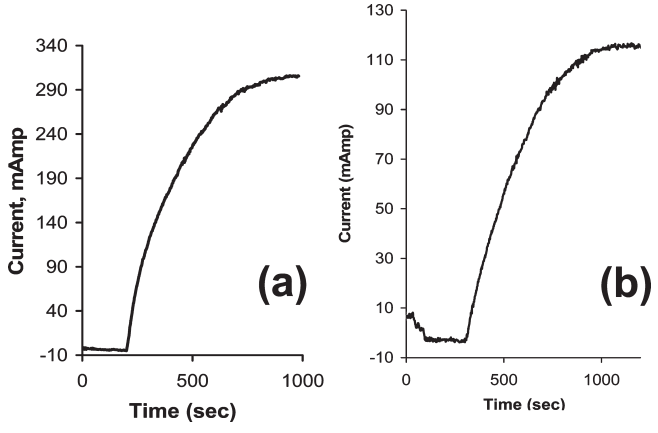

FIGURE 9: Oxygen evolution during peroxide reaction with WT and H135A-BSco. Profiles showing the increase in current upon the release of dioxygen during the reaction of (A) Cu(II)−WT BSco (800 μM) with 10 equiv of hydrogen peroxide. The maximum current produced (306 mA) corresponds to 367.2 μM O_2 (~38%). (B) Cu(II)−H135A-BSco (0.5 mM) with 1 equiv of hydrogen peroxide. The maximum current produced (116 mA) corresponds to 139.2 μM O_2 (~26%).

reaction with a rate constant k of 2.3 ± 1.2 M^{-1} s^{-1}, while H135A was reduced faster by 3 orders of magnitude with a rate constant of $(1.2 \pm 0.3) \times 10^3$ M^{-1} s^{-1}.

DISCUSSION

While it is clear that Sco1 is an essential accessory protein for Cu_A assembly, questions about whether it functions (1) as a simple metallochaperone for Cu(I) or Cu(II), (2) as a redox partner to maintain the two Cys residues in the Cu_A site in the reduced thiol(ate) form, or (3) in some more complex manner upstream of copper incorporation remain. H135 has been shown in this and other work to be essential to function, yet the data presented herein demonstrate that substitution of H135 with alanine does not result in elimination of copper binding but rather produces a variant with altered redox chemistry. Consideration of our results has allowed us to evaluate a new hypothesis for Sco function based on the idea that interaction of Sco with its partner might induce a conformational transition between His-on and His-off states at the copper center, providing a gated switch mechanism for converting the protein between active and inactive states. Here we evaluate our results with respect to both this and other more conventional mechanisms for Sco function.

As documented previously for yeast (*4*), human (*41*), *B. subtilis* (*2*), and more recently *Agrobacterium tumefaciens* (*42*), the H135A variant was inactive in cytochrome oxidase assembly. This work confirmed these earlier studies and further showed that this was not due to a lack of copper binding to BSco since H135A bound both Cu(II) and Cu(I) stoichiometrically. This finding contrasts previous reports from other laboratories where both yeast (H239A) and *B. subtilis* (H135A) Sco variants were reported to have a very low affinity for copper (*4*, *12*). EXAFS comparison of WT and H135A forms of the reduced enzyme shows little effect of removal of the H135 residue, with no evidence for imidazole outer shell scattering. The similarity between WT and H135A Cu(I) EXAFS confirms our previous analysis (*14*) that Cu(I)−WT BSco binds H135 at best in a substoichiometric fashion, providing evidence for His-on and His-off forms. The Cu(II)−H135A complex exhibits UV−vis spectra very similar to those of the WT protein, underscoring the dominance of Cu−S(Cys) charge transfer bands in the electronic spectra.

In contrast, EPR spectra show marked differences between WT and H135A. CW X-band EPR measurements of the Cu(II) form show that the N superhyperfine structure from the imidazole side chain of residue 135, which is clearly visible in the WT spectrum, is completely eliminated in the H135 variant, providing strong support for the loss of H135 coordination. EPR simulations identify both 1:1 and 2:1 imidazole adducts, neither of which matches the WT spectrum. Comparison of the g_z values for the 0:1, 1:1, and 2:1 imidazole complexes of H135A (Table 2) shows a clear trend of decreasing g_z as the number of imidazole groups is increased. The g_z value of the 1:1 imidazole complex is similar to that of WT and, as such, is consistent with a 1:1 N:Cu ligatation. However, other EPR parameters of the 1:1 complex differ significantly from those of the WT. Because two imidazoles can bind to the H135A mutant, there are two possible binding sites for the single imidazole in the 1:1 complex. The imidazole could bind at the same position as H135 in the WT, or it could bind at the fourth position which is believed to be occupied by an oxygen center ligand in the WT (*14*). The orientation of the anisotropic part of the nitrogen hyperfine matrix for the 1:1 imidazole complex is perpendicular to that of the WT [the maximum value of A_N is along y in WT but along x in the 1:1 imidazole adduct (Table 2)], suggesting that the imidazole does not bind at the native position of H135. Because the assignments of the x and y directions are rigorous only in single-crystal data, one cannot unambiguously determine the binding position of the exogenous imidazole ligand. It is also possible that the nominally 1:1 imidazole complex is actually a mixture of both isomers. These considerations argue that coordination of the 1:1 imidazole complex is different from that of the WT protein. It should also be noted that for the 2:1 imidazole complex the orientations of the two N hyperfine matrices are perpendicular to each other, which implies that the two exogenous imidazoles are cis to one another. This in turn implies that cysteines 45 and 49 are also cis to one another.

We also compared WT and H135A proteins with respect to their tendency toward Cu(II)−Cu(I)/cysteine-disulfide autoredox and their reactivity toward hydrogen peroxide. WT BSco is stable indefinitely in the Cu(II) form, although it was recently reported that the WT protein autoreduces to Cu(I) at high ionic strengths and in the presence of excess Cu(II) (*43*). In contrast, the Cu(II) centers of the H135A variant undergo rapid autoreduction at normal ionic strength in a process that appears to involve oxidation of C45 and C49 thiolates to a disulfide in one-third of the protein at the expense of reduction of two-thirds of the Cu(II) centers. Therefore, H135A stabilizes the Cu(II) center with respect to this autoredox process. A similar situation is found with peroxide reactivity. WT protein is slowly reduced by peroxide in a bimolecular (likely outer sphere) reaction, but the H135-substituted protein oxidizes peroxide in a rapid inner sphere reaction.

These data provide strong evidence that the Cu(II) form of Sco is essential to the function of the protein and argue against Sco functioning solely as a Cu(I) chaperone. First, the structure of the Cu(I) form is at best only slightly perturbed by the H135A substitution, yet function is eliminated. It also argues against a function as a redox partner to maintain the two Cys residues in the Cu_A site in the reduced thiol(ate) form. Our data clearly indicate that the role of H135 is to stabilize the Cu(II) form of the protein, yet crystallographic data show that an equilibrium between bis-thiol and disulfide forms occurs in the native BSco protein and does not require the presence of copper (*9*). Therefore, mechanisms based entirely on the reactivity of the two cysteine residues (C45 and C49) cannot explain the catastrophic effect of H135 substitution on function. Rather, our data establish an essential role of the Cu(II) form of Sco at some level in the reaction mechanism. The data do not rule out a possible chaperone role in which Sco must deliver copper in both oxidation states to the Cox2 polypeptide, which is reasonable given that Cu_A exists as a mixed-valence Cu(I)Cu(II) entity in its one-electron oxidized form. However, in light of these arguments, other less direct redox roles for Sco are also worthy of consideration.

Removal of the stabilizing histidine residue leads to a remarkable acceleration of peroxide reactivity and a change to saturation kinetics with respect to the peroxide substrate, suggesting direct binding of peroxide to a vacant coordination position on Cu(II). This observation may suggest that conformational changes in Sco to one in which the histidine is in an "off" position may act as a cellular target or sensor for hydrogen peroxide or other reductants. This situation is similar to the peroxidase activity exhibited by bacterial cytochrome *c* where the loss of an axial methionine either via mutation or due to unfolding of the

protein turns on the peroxidase activity (*44*). What makes this proposal of interest in this case is the fact that Sco NMR and crystal structures show that H135 resides on a loop which can take up variable conformations in both "Cu-on" and "Cu-off" conformations (*9*−*11*, *15*, *45*). Since exogenous imidazole binding does not appear to restore completely the spectral properties of Cu(II)−WT BSco, the inference is that H135 binds to the Cu(II) center in a unique configuration that imparts special stability on the Cu(II)−Sco structure. Conversely if the His-bearing loop is perturbed such that H135 no longer coordinates, the protein would become highly sensitive to reduction by hydrogen peroxide and other one-electron reductants such as Ti(III) citrate. Recent mutatgenesis studies have indeed implicated residues within this loop in a protein−protein interaction with the putative Sco1 partner Cox2 (*16*), and a loop-mediated Cox2 interaction could thus serve as a regulated redox switch.

Our studies implicate the copper center in the redox sensitivity of BSco. It is clear from many other investigations that the copper centers are important for maturation of the Cox2 protein. These include the ability of high levels of Sco to rescue the respiratory defect of *cox17-1* strains which harbor a mutation in a Cox17 copper binding ligand (*1*), Sco variants with mutations in the copper binding ligands which all abrogate Cox2 assembly (*2*, *4*, *41*), and variants such as human Sco P74L which disrupt the interaction interface of copper from Cox17 to Sco (*46*). However, direct transfer of copper from Sco to Cox2 has not been demonstrated. In *T. thermophilus*, Sco was found to be unable to transfer copper to Cox2 under conditions where transfer proceeded in a facile manner from the periplasmic copper binding protein PCuAC (*7*). Similar results were obtained in our hands where Cu-loaded BSco was capable of less than 20% reconstitution of *B. subtilis* Cox2 (Ctac) in vitro (data not shown). It is therefore likely that Sco assists in the metalation of the Cu_A center by some indirect pathway, perhaps involving peroxide or more generally redox reactivity.

In yeast, WT Sco1 confers peroxide resistance as evidenced by the observation that *sco1*Δ strains show increased sensitivity to hydrogen peroxide (*47*). This sensitivity maps to the loop that carries the copper−histidine ligand, H239 in yeast (pink loop of BSco in Figure 10) (*16*). The observation that these loop-directed substitutions abrogate the ability of Sco1 to suppress the respiratory defect of Cox17-1 cells suggests that it is the interaction with Cox2 that is disrupted, rather than with Cox17. However, Sco1 variants harboring copper site mutations (C148A and C152A) are peroxide resistant, while WT human Sco1 confers peroxide resistance in yeast without rescuing the respiratory defect of *sco1*Δ strains. The protective effect of Sco1 cannot therefore be due to redox activity at the copper center. The mechanism of peroxide sensitivity has been traced to the transient accumulation of a heme a_3 pro-oxidant in the immature Cox1 subunit (*47*), and it has been suggested that Sco-mediated peroxide resistance involves binding of a Sco−Cox2 complex to the nascent Cox1 which occludes entry of peroxide into a channel which leads to the heme a_3−Cu_B dioxygen binding site. In Sco1 variants where the Sco1−Cox2 interface is disrupted, binding does not occur, leading to facile access of peroxide to the Cox1−heme a_3 center with potential formation of ferryl-type high-valent intermediates.

While peroxide resistance cannot involve redox reactions at the copper center, the involvement of redox chemistry within a Cox1−Sco1−Cox2 complex is worth further consideration (Figure 10). In the absence of high fluxes of hydrogen peroxide, the immature Cox1 subunit may still generate the high-valent intermediates P and F (Figure 10) in which the O−O bond is broken. However, the electrons necessary to complete the reaction cycle derived from cytochrome *c* are fed into the reactive binuclear site via the redox-coupled Fe_a−Cu_A metal centers. Since Cox2 is the final subunit to be assembled, it follows that the immature oxidase lacking Cox2 will be vulnerable to buildup of high-valent intermediates, since these electrons will be

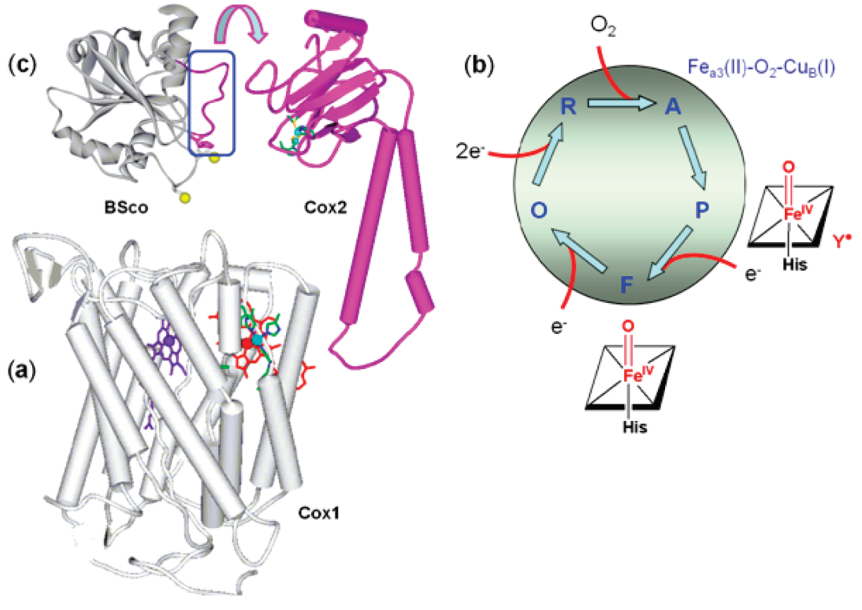

FIGURE 10: Possible mechanism for the function of Sco. (a) Subunit 1 (Cox1) of cytochrome *c* oxidase. The structure is taken from Protein Data Bank entry 1QLE. (b) The catalytic reduction of dioxygen to water by cytochrome *c* oxidase cycles through various dioxygen intermediates. The steps from R through F can occur using electrons stored in the reduced subunit 1 metal centers and can therefore proceed prior to subunit 2 insertion. The final conversion of F to O requires donation of an electron from subunit 2 (Cox2). Therefore, high-valent intermediates could conceivably build up in Cox1 from reaction with dioxygen prior to Cox2 assembly. (c) Interaction between subunit 2 and Sco via mobile loop 8 (pink) of Sco. This may allow docking of a Sco−Cox2 complex with Cox1 facilitating oxidation of the Cox1 metal centers, thereby protecting the enzyme from oxidative damage.

unavailable. In particular, if the binuclear Fe_a-Cu_B center is present in its reduced form, high-valent intermediates can accumulate from reaction with molecular oxygen. This analysis suggests that it is important to control the redox state of Cox1 during the assembly process. Given the evidence for interaction of Sco1 both with Cox1 (*47*) and with Cox2 (*16*), it is plausible that Sco1 might serve a redox buffering role, perhaps by accepting electrons from the reduced or semireduced binuclear center, thereby preventing oxygen reactivity until Cox2 was fully integrated into the complex. This would imply a role for the Cu(II) form of Sco, which would be reduced to its Cu(I) form in the process. Whether the resulting Cu(I) center is transferred to Cu_A is an open question. On the other hand, quinol oxidases such as the *B. subtilis* aa_3-600 or *E. coli* bo_3 do not appear to require Sco for assembly, even though similar P and F intermediates form in subunit 1. It is possible that in these cases the hydroquinol electron donors are capable of fulfilling the proposed redox buffering function.

In conclusion, our observations point to an essential role of the Cu(II) form of Sco at some level in the reaction mechanism. Whether this role involves reductive stabilization of Cox1, direct transfer of Cu(II) to the Cu_A center to form the mixed-valence species, or some alternative function remains to be determined.

ACKNOWLEDGMENT

We thank Dr. Martina Ralle for mass spectrometery measurements.

SUPPORTING INFORMATION AVAILABLE

Supporting Information (eight figures and two tables). This material is available free of charge via the Internet at http://pubs.acs.org.

REFERENCES

1. Glerum, D. M., Shtanko, A., and Tzagoloff, A. (1996) SCO1 and SCO2 act as high copy suppressors of a mitochondrial copper recruitment defect in *Saccharomyces cerevisiae*. *J. Biol. Chem. 271*, 20531–20535.
2. Mattatall, N. R., Jazairi, J., and Hill, B. C. (2000) Characterization of YpmQ, an accessory protein required for the expression of cytochrome *c* oxidase in *Bacillus subtilis*. *J. Biol. Chem. 275*, 28802–28809.
3. Bengtsson, J., von Wachenfeldt, C., Winstedt, L., Nygaard, P., and Hederstedt, L. (2004) CtaG is required for formation of active cytochrome *c* oxidase in *Bacillus subtilis*. *Microbiology 150*, 415–425.
4. Nittis, T., George, G. N., and Winge, D. R. (2001) Yeast Sco1, a protein essential for cytochrome *c* oxidase function is a Cu(I)-binding protein. *J. Biol. Chem. 276*, 42520–42526.
5. Lode, A., Kuschel, M., Paret, C., and Rodel, G. (2000) Mitochondrial copper metabolism in yeast: Interaction between Sco1p and Cox2p. *FEBS Lett. 485*, 19–24.
6. Leary, S. C., Kaufman, B. A., Pellecchia, G., Guercin, G. H., Mattman, A., Jaksch, M., and Shoubridge, E. A. (2004) Human SCO1 and SCO2 have independent, cooperative functions in copper delivery to cytochrome c oxidase. *Hum. Mol. Genet. 13*, 1839–1848.
7. Abriata, L. A., Banci, L., Bertini, I., Ciofi-Baffoni, S., Gkazonis, P., Spyroulias, G. A., Vila, A. J., and Wang, S. (2008) Mechanism of Cu(A) assembly. *Nat. Chem. Biol. 4*, 599–601.
8. Chinenov, Y. V. (2000) Cytochrome c oxidase assembly factors with a thioredoxin fold are conserved among prokaryotes and eukaryotes. *J. Mol. Med. 78*, 239–242.
9. Ye, Q., Imriskova-Sosova, I., Hill, B. C., and Jia, Z. (2005) Identification of a disulfide switch in BsSco, a member of the Sco family of cytochrome *c* oxidase assembly proteins. *Biochemistry 44*, 2934–2942.
10. Williams, J. C., Sue, C., Banting, G. S., Yang, H., Glerum, D. M., Hendrickson, W. A., and Schon, E. A. (2005) Crystal structure of human SCO1: Implications for redox signaling by a mitochondrial cytochrome c oxidase "assembly" protein. *J. Biol. Chem. 280*, 15202–15211.
11. Banci, L., Bertini, I., Calderone, V., Ciofi-Baffoni, S., Mangani, S., Martinelli, M., Palumaa, P., and Wang, S. (2006) A hint for the function of human Sco1 from different structures. *Proc. Natl. Acad. Sci. U.S.A. 103*, 8595–8600.
12. Imriskova-Sosova, I., Andrews, D., Yam, K., Davidson, D., Yachnin, B., and Hill, B. C. (2005) Characterization of the redox and metal binding activity of BsSco, a protein implicated in the assembly of cytochrome *c* oxidase. *Biochemistry 44*, 16949–16956.
13. Badrick, A. C., Hamilton, A. J., Bernhardt, P. V., Jones, C. E., Kappler, U., Jennings, M. P., and McEwan, A. G. (2007) PrrC, a Sco homologue from *Rhodobacter sphaeroides*, possesses thiol-disulfide oxidoreductase activity. *FEBS Lett. 581*, 4663–4667.
14. Andruzzi, L., Nakano, M., Nilges, M. J., and Blackburn, N. J. (2005) Spectroscopic studies of metal binding and metal selectivity in *Bacillus subtilis* BSco, a homologue of the yeast mitochondrial protein Sco1p. *J. Am. Chem. Soc. 127*, 16548–16558.
15. Balatri, E., Banci, L., Bertini, I., Cantini, F., and Ciofi-Baffoni, S. (2003) Solution structure of Sco1: A thioredoxin-like protein involved in cytochrome *c* oxidase assembly. *Structure 11*, 1431–1443.
16. Rigby, K., Cobine, P. A., Khalimonchuk, O., and Winge, D. R. (2008) Mapping the functional interaction of Sco1 and Cox2 in cytochrome oxidase biogenesis. *J. Biol. Chem. 283*, 15015–15022.
17. Guerout-Fleury, A. M., Shazand, K., Frandsen, N., and Stragier, P. (1995) Antibiotic-resistance cassettes for *Bacillus subtilis*. *Gene 167*, 335–336.
18. Britton, R. A., Eichenberger, P., Gonzalez-Pastor, J. E., Fawcett, P., Monson, R., Losick, R., and Grossman, A. D. (2002) Genome-wide analysis of the stationary-phase sigma factor (sigma-H) regulon of *Bacillus subtilis*. *J. Bacteriol. 184*, 4881–4890.
19. Le Brun, N. E., Bengtsson, J., and Hederstedt, L. (2000) Genes required for cytochrome *c* synthesis in *B. subtilis*. *Mol. Microbiol. 36*, 638–650.
20. Carter, P. (1987) Improved oligonucleotide-directed mutagenesis using m13 vectors. *Methods Enzymol. 154*, 382–403.
21. Nelson, D. P., and Kiesow, L. A. (1972) Enthalpy of decomposition of hydrogen peroxide by catalase at 25 °C (with molar extinction coefficients of H_2O_2 solutions in the UV). *Anal. Biochem. 49*, 474–478.
22. Bauman, A. T., Yukl, E. T., Alkevich, K., McCormack, A. L., and Blackburn, N. J. (2006) The hydrogen peroxide reactivity of peptidylglycine monooxygenase supports a Cu(II)-superoxo catalytic intermediate. *J. Biol. Chem. 281*, 4190–4198.
23. Uppal, R., Incarvito, C. D., Lakshmi, K. V., and Valentine, A. M. (2006) Aqueous spectroscopy and redox properties of carboxylate-bound titanium. *Inorg. Chem. 45*, 1795–1804.
24. Kuzmic, P. (1996) Program DYNAFIT for the analysis of enzyme kinetic data: Application to HIV proteinase. *Anal. Biochem. 237*, 260–273.
25. Nilges, M. J., Matteson, K., and Belford, R. L. (2006) in ESR Spectroscopy in Membrane Biophysics (Hemminga, M. A., and Berliner, L. J., Eds.) Springer, New York.
26. Barry, A. N., and Blackburn, N. J. (2008) A selenocysteine variant of the human copper chaperone for superoxide dismutase. A Se-XAS probe of cluster composition at the domain 3-domain 3 dimer interface. *Biochemistry 47*, 4916–4928.
27. George, G. N. (1995) EXAFSPAK, Stanford Synchrotron Radiation Laboratory, Menlo Park, CA.
28. Binsted, N., and Hasnain, S. S. (1996) State of the art analysis of whole X-ray absorption spectra. *J. Synchrotron Radiat. 3*, 185–196.
29. Binsted, N., Gurman, S. J., and Campbell, J. W. (1998) EXCURVE, version 9.2, Daresbury Laboratory, Warrington, England.
30. Blackburn, N. J., Rhames, F. C., Ralle, M., and Jaron, S. (2000) Major changes in copper coordination accompany reduction of peptidylglycine monooxygenase. *J. Biol. Inorg. Chem. 5*, 341–353.
31. Fann, Y. C., Ahmed, I., Blackburn, N. J., Boswell, J. S., Verkhovskaya, M. L., Hoffman, B. M., and Wikstrom, M. (1995) Structure of Cu_B in the binuclear heme-copper center of the cytochrome aa_3-type quinol oxidase from *Bacillus subtilis*. *Biochemistry 34*, 10245–10255.
32. Solomon, E. I., Szilagyi, R. K., DeBeer George, S., and Basumallick, L. (2004) Electronic structures of metal sites in proteins and models: Contributions to function in blue copper proteins. *Chem. Rev. 104*, 419–458.
33. John, E., Bharadwaj, P. K., Potenza, J. A., and Schugar, H. J. (1986) Characterization of [*rac*-5,7,7,12,14,14-hexamethyl-1,4,8,11-tetraazacyclotetradecane]copper(II) 3-sulfidopropionate dimethanolate, $[Cu(tet\ b)SCH_2CH_2CO_2]\cdot 2CH_3OH$, a stable copper(II)-aliphatic thiolate complex. *Inorg. Chem. 25*, 3065–3069.
34. Stibrany, R. T., Fikar, R., Brader, M., Potenza, M. N., Potenza, J. A., and Schugar, H. J. (2002) Charge-transfer spectra of structurally characterized mixed-valence thiolate-bridged Cu(I)/Cu(II) cluster complexes. *Inorg. Chem. 41*, 5203–5215.

35. Basumallick, L., Sarangi, R., DeBeer George, S., Elmore, B., Hooper, A. B., Hedman, B., Hodgson, K. O., and Solomon, E. I. (2005) Spectroscopic and density functional studies of the red copper site in nitrosocyanin: Role of the protein in determining active site geometric and electronic structure. *J. Am. Chem. Soc. 127*, 3531–3544.
36. Arciero, D. M., Pierce, B. S., Hendrich, M. P., and Hooper, A. B. (2002) Nitrosocyanin, a red cupredoxin-like protein from *Nitrosomonas europaea*. *Biochemistry 41*, 1703–1709.
37. Lieberman, R. L., Arciero, D. M., Hooper, A. B., and Rosenzweig, A. C. (2001) Crystal structure of a novel red copper protein from *Nitrosomonas europaea*. *Biochemistry 40*, 5674–5681.
38. Pickering, I. J., George, G. N., Dameron, C. T., Kurz, B., Winge, D. R., and Dance, I. G. (1993) X-ray absorption spectroscopy of cuprous-thiolate clusters in proteins and model systems. *J. Am. Chem. Soc. 115*, 9498–9505.
39. Badrick, A. C., Hamilton, A. J., Bernhardt, P. V., Jones, C. E., Kappler, U., Jennings, M. P., and McEwan, A. G. (2007) PrrC, a Sco homologue from *Rhodobacter sphaeroides*, possesses thiol-disulfide oxidoreductase activity. *FEBS Lett. 581*, 4663–4667.
40. Banci, L., Bertini, I., Ciofi-Baffoni, S., Leontari, I., Martinelli, M., Palumaa, P., Sillard, R., and Wang, S. (2007) Human Sco1 functional studies and pathological implications of the P174L mutant. *Proc. Natl. Acad. Sci. U.S.A. 104*, 15–20.
41. Horng, Y. C., Leary, S. C., Cobine, P. A., Young, F. B., George, G. N., Shoubridge, E. A., and Winge, D. R. (2005) Human Sco1 and Sco2 function as copper-binding proteins. *J. Biol. Chem. 280*, 34113–34122.
42. Saenkham, P., Vattanaviboon, P., and Mongkolsuk, S. (2009) Mutation in *sco* affects cytochrome *c* assembly and alters oxidative stress resistance in *Agrobacterium tumefaciens*. *FEMS Microbiol. Lett. 293*, 122–129.
43. Davidson, D. E., and Hill, B. C. (2009) Stability of oxidized, reduced and copper bound forms of *Bacillus subtilis* Sco. *Biochim. Biophys. Acta 1794*, 275–281.
44. Worrall, J. A., Diederix, R. E., Prudencio, M., Lowe, C. E., Ciofi-Baffoni, S., Ubbink, M., and Canters, G. W. (2005) The effects of ligand exchange and mobility on the peroxidase activity of a bacterial cytochrome c upon unfolding. *ChemBioChem 6*, 747–758.
45. Abajian, C., and Rosenzweig, A. C. (2006) Crystal structure of yeast Sco1. *J. Biol. Inorg. Chem. 11*, 459–466.
46. Cobine, P. A., Pierrel, F., Leary, S. C., Sasarman, F., Horng, Y. C., Shoubridge, E. A., and Winge, D. R. (2006) The P174L mutation in human Sco1 severely compromises Cox17-dependent metallation but does not impair copper binding. *J. Biol. Chem. 281*, 12270–12276.
47. Khalimonchuk, O., Bird, A., and Winge, D. R. (2007) Evidence for a pro-oxidant intermediate in the assembly of cytochrome oxidase. *J. Biol. Chem. 282*, 17442–17449.